European Journal of Pharmaceutical Sciences 146 (2020) 105267

Contents lists available at ScienceDirect

European Journal of Pharmaceutical Sciences

journal homepage: www.elsevier.com/locate/ejps

Preparation and characterization of a new solid form of praziquantel, an essential anthelmintic drug. Praziquantel racemic monohydrate

Duvernis Salazar-Rojas, Rubén M. Maggio*, Teodoro S. Kaufman

Pharmaceutical Analysis, Department of Organic Chemistry, School of Pharmaceutical and Biochemical Sciences, National University of Rosario and Institute of Chemistry of Rosario (IQUIR, CONICET-UNR), Suipacha 531, Rosario, S2002LRK, Argentina

ARTICLE INFO

Keywords:
Racemic praziquantel
Monohydrate
Pseudo-polymorphism
Solid-state characterization
Vibrational spectroscopy
DSC and TGA

ABSTRACT

Praziquantel (PZQ) is a highly effective low-cost anthelmintic agent used as the first-choice treatment against schistosomiasis. The low solubility of the active is a major drawback for pharmaceutical formulation. A valid approach of the pharmaceutical industry for the improvement of the pharmacotechnical features of the active principles (such as solubility, processability, stability, among others), is the preparation of new solid forms, such as salts, polymorph, and pseudo-polymorph.

Herein we report the preparation and characterization of a new solid form PZQ. The PZQ monohydrate (PZQ-MH) was prepared by a solventless procedure from the commercial racemate and the product was characterized at the solid-state employing optical digital microscopy, thermal methods (melting point, differential scanning calorimetry and thermogravimetric analysis), as well as and mid-infrared and near infrared spectroscopies. The chemical structure and content of water were full assessed by ^{1}H nuclear magnetic resonance (NMR) in solution. The amount of water in PZQ-was also determined by different approaches, including thermogravimetric analysis and the loss on drying test. Solid-state ^{13}C NMR (ssNMR) and X-ray powder diffraction (XRPD) completed the structural characterization of the new monohydrate.

PZQ-MH showed a crystalline behavior during XRPD experiments and showed relevant differences in spectroscopic, calorimetric, ssNMR and XRPD signals when it was compared with the known crystal (Form A) and amorphous forms of PZQ. The determination of the intrinsic dissolution rate (IDR) of PZQ-MH was carried out as a functional characterization, observing that the new form had slightly higher IDR than Form A.

1. Introduction

Praziquantel (PZQ, Fig. 1) is (11b-*RS*) − 2-cyclohexylcarbonyl-1,2,3,6,7-hexahydro-4*H*-pyrazino[2,1-*a*]isoquinolin-4-one (da Silva et al., 2017; El-subbagh and Al-badr, 1998). This essential drug is the first-choice anti-parasitic against schistosomiasis (also known as snail fever or bilharziasis), a socioeconomically devastating chronic helminth infection caused by trematodes of the genus *Schistosoma* (Kolenyak-Santos et al., 2015), particularly by *S. mansoni* (Coeli et al., 2013). According to the World Health Organization, this neglected disease affects 230 million people worldwide and causes an annual death toll of over 5 million, being the third cause of morbidity by tropical disease (World Health Organization, 2019).

PZQ has been used to treat a wide variety of helminth infections in both, humans and animals (Bygott and Chiodini, 2009; Liu et al., 2004). PZQ proved to be effective against all forms of schistosomiasis and no therapeutic alternatives to the drug are currently available (Mari et al., 2017). Moreover, PZQ is the only active pharmaceutical ingredient (API) indicated for the treatment of opisthorchiasis (Meister et al., 2016), as well as the drug of choice in human taeniasis. In addition, PZQ has low cost, high efficacy, high tolerance and minor side effects in comparison to other anti-parasite drugs; however, its poor bio-availability is one of the weak points (Borrego-Sánchez et al., 2016).

PZQ is classified as a Class II API in the Biopharmaceutics Classification System, because of its low water solubility (0.04 mg/mL) and high permeability across biological membranes (Borrego-Sánchez et al., 2016; Gonzales-Esquivel et al., 2005); the latter markedly affects the dissolution process, and its therapeutic efficiency, as a result of limiting drug bioavailability.

Polymorphism emerges as one of the valid alternatives to improve some properties of pharmaceutical solids, without the introduction of exogenous atoms or molecules in the API structure. The same is true for pseudo-polymorphs, which in some cases are preferred for manufacturing purposes (Blanco et al., 2005), especially when the anhydrate

* Corresponding author.
E-mail address: maggio@iquir-conicet.gov.ar (R.M. Maggio).

https://doi.org/10.1016/j.ejps.2020.105267
Received 10 July 2019; Received in revised form 18 December 2019; Accepted 11 February 2020
Available online 13 February 2020
0928-0987/

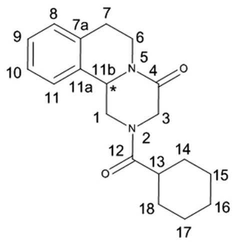

Fig. 1. Chemical structure of PZQ. Atom numbering is according to (da Silva et al., 2017) and the asterisk indicates the position of the stereogenic center.

lacks proper crystal morphology (Witzleb et al., 2011) or holds high hygroscopicity.

Despite, it is being used for human treatment since early in ’80s or before (Bylund et al., 1977; Leopold et al., 1978) not many research groups have paid attention to solid-state properties of PZQ and the formation of new solid phases. This lack of interest may stem from the low cost of PZQ (Management Sciences for Health and World Health Organization, 2011) or the rare incidence of its side effects (World Health Organization, 2008), which do not prevent to use higher-doses when needed. Thus the availability of information about solid phase variations of PZQ is rather scarce.

A few reports on the preparation of PZQ co-crystals with a variety of carboxylic acids (Espinosa-Lara et al., 2013), the design of solid dispersions with sodium starch glycolate (Chaud et al., 2013), poly(vinylpyrrolidone)-based formulations (Costa et al., 2016) and cyclodextrin complexes (Cugovcan et al., 2017), could be listed as the most relevant works in this field. Racemic PZQ has two reported crystal forms and an amorphous form. PZQ-A (the form present in commercial APIs) is obtained as a needle-like crystalline anhydrate (Espinosa-Lara et al., 2013). The crystals of this form are a racemate [(R/S)-PZQ, CSD-TELCEU-896767], where each unit cell contains two pairs of both enantiomers of the drug and the carbonyl motifs are in a *syn* conformation. The recently reported form B (PZQ-B), prepared under solventless condition, contains one independent molecule in the unit cell and it has been proposed that the carbonyl moieties are in the *anti*-conformation (Borrego-Sánchez et al., 2016; Borrego-Sanchez, 2018). Finally, based on the analysis of solid-state nuclear magnetic resonance (ssNMR) spectra, Arrúa et al. suggested that the carbonyl moieties of the amorphous form (PZQ-AM) should be predominantly in an *anti*-conformation (Arrúa et al., 2015; Costa et al., 2016)

In addition, the pure (*R*)- and (*S*)- enantiomers of the drug have been obtained and their single-crystal X-ray diffraction analysis revealed that they are packed with the carbonyls in an *anti* conformation (Cedillo-Cruz, 2013). PZQ optically pure (*R*)- enantiomer was further converted into the corresponding crystalline hemihydrate (Meyer et al., 2009). It is also worth mentioning that in the last years, an effort to prepare others solids forms of racemic PZQ has been made by slow evaporation of the drug solutions from several solvents, however, it failed and only the original crystal form was obtained (Toro et al., 2014)

Knowledge of the relevant solid-state properties, as well as physicochemical and functional properties of APIs, is a key step toward achieving better medicines. Hence, the search for solid-state varieties of pharmacologically relevant solids is a permanent topic of major interest. With the intention to expand the landscape of PZQ solid state and in order to improve its pharmaceutical properties, herein we report the preparation and characterization of a hitherto unknown hydrate of PZQ racemate, namely the monohydrate (PZQ-MH). Furthermore, the results of comparative dissolution studies of PZQ-MH against PZQ-A and PZQ-AM revealed a slight improvement in dissolution profile of PZQ-MH over PZQ-A.

2. Materials and methods

2.1. Instrumentation and software

The medium infrared (MIR) spectra were acquired in a Shimadzu Prestige 21 FTIR spectrometer (Shimadzu Corp., Kyoto, Japan), in the absorbance mode (20 scans each), over a wavenumber range of 4000–600 cm^{-1} and at a resolution of 4 cm^{-1}. The ATR experiments were carried out with a diamond-based ATR accessory (GladiATR, Pike Technologies, Madison, USA), fitted with a Pike temperature control unit. Samples were measured in triplicate.

The near-infrared (NIR) spectra were measured at room temperature in the reflectance mode with a FOSS NIRS DS2500 spectrometer (FOSS, Hilleroed, Denmark) in the spectral range 700–2500 nm. The determinations were carried out in triplicate, with the samples (700 mg) placed in a circular quartz cell for solids.

The differential scanning calorimetric (DSC) determinations were executed with a Linseis model PT1000 (Linseis, Selb, Germany) instrument. The samples (3–5 mg) were placed in closed unsealed aluminum pans, to equilibrate pressures. The pans were heated at 2 °C min^{-1} between 30 °C and 120 °C and then at 10 °C min^{-1} up to 170 °C under a constant flow of nitrogen (50 mL min^{-1}). An empty aluminum pan was used as a reference.

The thermogravimetric analyses (TGA) were conducted on a Shimadzu DTG-60H (Shimadzu, Kyoto, Japan) instrument, with a nitrogen purge of 30 mL min^{-1}. During each analysis, about 10 mg of the sample was heated at a rate of 10 °C min^{-1} between 30 °C and 170 °C. An empty aluminum pan was used as a reference.

The melting points were determined with an Ionomex melting point instrument (Ionomex, Buenos Aires, Argentina). The samples were heated at 10 °C min^{-1} up to 130 °C; then, the heating rate was changed to 1 °C min^{-1} until past the melting event.

The digital optical microscopy of the crystal forms was carried out with the aid of an optical microscope (Seiwa Optical, Tokyo, Japan), fitted with 10×, 40 × and 100 × objectives and a 4 × 5.0 megapixels [resolution 2592 × 1944 (*H* × *V*)] Beion CMOS digital camera (Shanghai Beion Medical Technology Co., Ltd., Shanghai, China).

The dissolution tests were carried out using a Hanson SR8-Plus dissolution station (Hanson Research, Chatsworth, USA), configured as USP apparatus II (paddles) (U.S. Pharmacopeial Convention, 2015).

The UV–Vis spectroscopic determinations were performed in an Agilent 8453 UV–DAD spectrophotometer (Agilent Technologies, Santa Clara, USA), using a quartz cell (10 mm optical path length) against a blank of the solvent.

The ^{1}H nuclear magnetic resonance (NMR) spectra were acquired at 300 MHz in a Bruker Avance 300 spectrometer (Bruker BioSpin GmbH, Karlsruhe, Germany) with the samples dissolved in anhydrous $CDCl_3$ and using tetramethylsilane (TMS) as internal standard.

The ^{13}C ssNMR spectra were acquired with the cross-polarization at the magic angle spinning technique (CP/MAS), at 100 MHz in a Bruker Avance 400 spectrometer. The ^{13}C spinning sidebands were suppressed using the TOSS (Total Suppression of Spinning Sidebands) sequence. The solid samples (approx. 20 mg) were powdered in a mortar, placed in standard zirconium rotors (ZiO_2) and sealed with Kel-F caps. The spinning rate was set at 7 kHz, the contact time during cross-polarization was 2 ms, and the relaxation time was 5 s. The chemical shifts (δ) are reported in ppm downfield from TMS; coupling constants (*J*) are expressed in Hz. All NMR spectra were acquired and analyzed using Topspin v.3.5 (Bruker); for further analysis and processing, data were exported in ASCII format.

X-ray powder diffraction (XRPD) patterns were obtained using a Panalytical MPD unit equipped with a Cu anode, X-ray lenses, Xe gas detector, graphite monochromator and Soller parallel plates on the secondary beam. Measurements were made adding the Kα1,2 signals, with vertical and horizontal slits (3 × 3 mm^2 beam area), in continuous scans (5 s per 0.02° 2θ increment) in the 20° < 2θ < 105° range.

Graphs of the analytical signals were executed in OriginPRO v.8 (OriginLab, Northampton, USA) from their original data in ASCII format. The chemical structure was drawn using the ChemOffice Pro-v.16 software (Perkin Elmer Informatics, Cambridge, USA).

2.2. Chemicals and reagents

PZQ (USP grade) bulk drug was acquired from Unifarma S.A. (Buenos Aires, Argentina) and kept in a desiccator protected from the light. Commecial PZQ demonstrated to be a racemic mixture ($[\alpha]_D^{25}$ = +0.95 ± 1.20, n = 5, c = 1, $CHCl_3$) and confirmed to be polymorph A (XRPD). All solvents used were of analytical grade.

2.3. Preparation of the solid forms of PZQ

PZQ-A was obtained by dissolving racemic commercial PZQ (100 mg) in acetone (50 mL) at room temperature, heating this solution to 50 °C and adding more PZQ (380 mg) to obtain a supersaturated solution. The undissolved drug was removed by filtration and the filtrate was slowly concentrated by solvent evaporation at room temperature.

PZQ-AM was obtained as a highly hygroscopic glass, using a slight modification of the literature procedure (Costa et al., 2016). PZQ-A (300 mg) was weighed in a stainless-steel container and placed in a vacuum oven at 150 °C and 60 mmHg during 30 min; then, the molten drug in the container was transferred to a desiccator and left to reach room temperature. The obtained solid was finally stored below the 30 °C in tightly closed caramel flasks.

PZQ-MH was prepared by weighing PZQ-A (300 mg) in a stainless-steel container and melting the solid in a vacuum oven at 150 °C and 60 mmHg during 30 min. Then, the stainless-steel container with the melt was transferred to a humidity temperature-controlled chamber (Fig. 2). The molten solid was whisked using a stainless paddle (100 rpm) while rapidly being cooled with liquid nitrogen in under controlled temperature and humidity conditions (20 °C and over 70% RH). The so obtained solid was kept in a freezer (−20 °C) overnight, before being finally stored below 30 °C in tightly closed caramel flasks.

2.4. Determination of the intrinsic dissolution rate of the solid-state forms

The intrinsic dissolution rate (IDR) of different PZQ forms was determined from tablets, obtained by direct compression of the corresponding powders with a hydraulic press (Perkin Elmer, Norwalk, USA). For tablet preparation, the samples (150 mg) were placed in a Teflon® pan that served as sample holder (I.D. = 13 mm) and subjected to a pressure of 2 T cm^{-2} for 2 min. The resulting tablets had a flat surface area of 1.327 cm^2.

The dissolutions were performed in previously degassed double-distilled water (1000 mL), at 37 °C and a paddle rotation rate of 100 rpm. Aliquots of 3 mL were withdrawn with replacement, at pre-established times (5, 10, 20, 30, 40, 50, and 60 min) and the amount of dissolved PZQ was determined spectroscopically at 220 nm. A correction was applied for the cumulative dilution caused by the addition of the fresh dissolution medium.

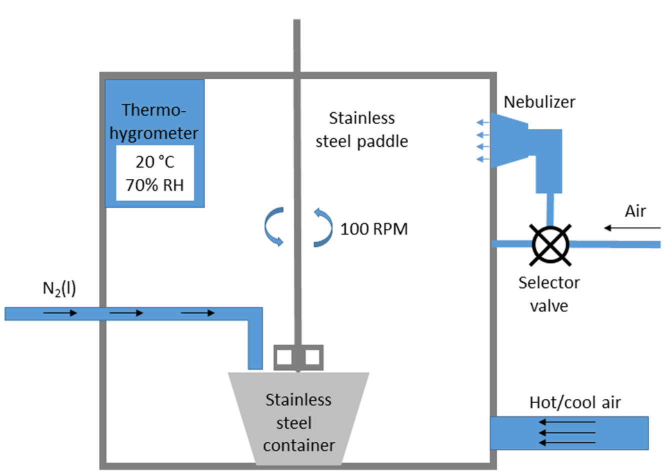

Fig. 2. Instrumental layout for the preparation of PZQ-MH.

3. Results and discussion

The new solid form of the drug prepared as described in section 2.3 were characterized at the solid-state and compared with known forms, employing different concurrent means, including microscopy, thermal analysis, vibrational spectroscopy (MIR/NIR), ssNMR, XRPD and a functional test. The presence of water was assessed by various methodologies.

3.1. Confirmation of the chemical structure of the new species. Assessment of the presence of water in the hydrate

^{1}H NMR spectroscopy is able to reveal the chemical structure of the analytes, as well as their chemical changes, including hydrogen exchange rate by providing information on the chemical environment of its sensitive nuclei. Fig. 3 shows the solution ^{1}H NMR spectra of the studied forms; they exhibited high degree of similarity and those of PZQ-A and PZQ-AM were congruent and in agreement with the literature (Woelfle et al., 2011). No additional resonances were found, confirming that no significant degradation took place during the melting and crystallization procedures.

The duplicated signals for methylenic and methinic carbons are due to the presence of a rotameric equilibrium between its anti and syn conformers of PZQ in solution, as reported by Meyer et al. (2009).

A more in-depth spectral comparison revealed that all the forms exhibited the same spectroscopic pattern in the range δ 2.0–7.5 ppm. However, in the upfield zone (δ 1.0–2.0 ppm), it was detected that PZQ-MH exhibited an additional and easily distinguished resonance around δ 1.63 ppm, which was assigned to H_2O. When the integral of this signal was compared with that of the doublets resonating in the 4.6–3.7 ppm region (assigned to both protons attached to C-3), it was found that the areas were comparable in size. Hence, it was concluded that the stoichiometry of PZQ-MH should be PZQ.H_2O.

The chemical shift of this singlet was significantly different from that found for moisture as a solvent impurity in $CDCl_3$ (δ 1.56 ppm)

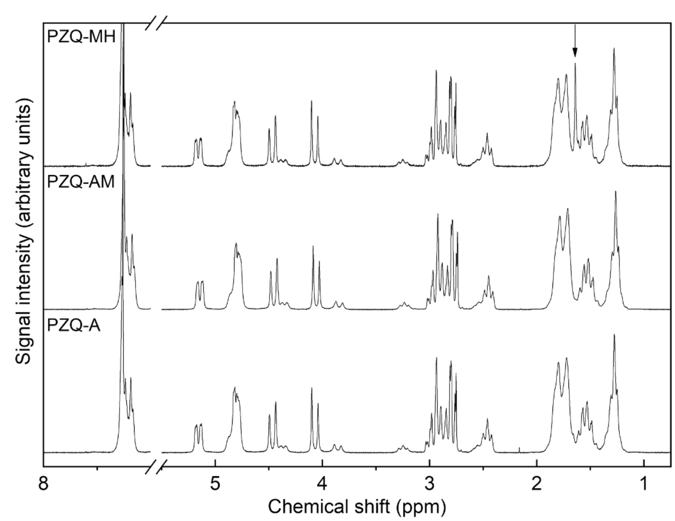

Fig. 3. ^{1}H NMR spectra of the different forms of PZQ in anhydrous $CDCl_3$. The arrow points to the signal of water.

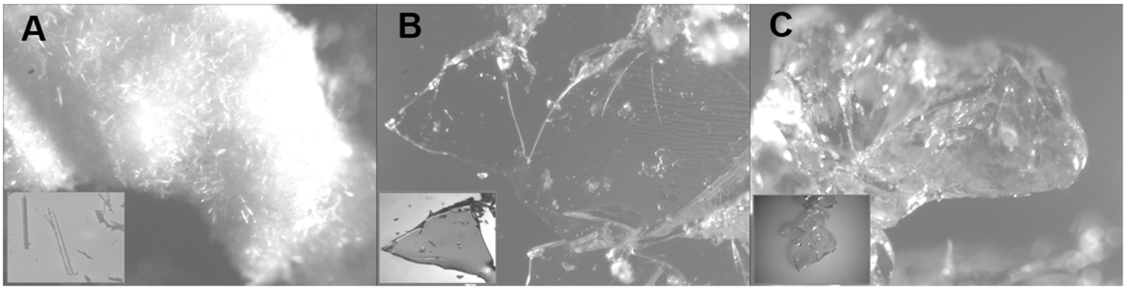

Fig. 4. Digital optical microscopy images of the solids (conglomerates) at a magnification of 40 × . (A) PZQ-A; (B) PZQ-AM and (C) PZQ-MH. Separated crystals of the solids forms (bottom left) at a magnification of 400 × (40 × optical * 10 × digital).

(Gottlieb et al., 1997), possibly reflecting its interaction with PZQ. The exchangeable nature of these protons was assessed by addition of D_2O (Tode et al., 2009), which resulted in the disappearance of the δ 1.63 ppm peak. Hence, the new signal found in PZQ-MH could be unequivocally attributed to hydration water, providing the first confirmation on the presence of a hitherto unknown monohydrate of PZQ.

3.2. Microscopic and macroscopic analysis

The digital optical microscopy images of the different solid forms of PZQ are displayed in Fig. 4. The major features of the crystallization habit of recrystallized PZQ-A were isolated white needles and white acicular groups of needle-like crystals. On the other hand, in agreement with the expectations for an amorphous form, PZQ-AM showed poorly defined forms, and no habits were found after powdering of the solid.

In addition, PZQ-MH was seen as a pink solid with small particle size, but still lacking a well-defined habit. It was conjectured that the observed color in PZQ-MH may be the result of intermolecular interactions, since when the solid was heated a smooth conversion into whitish solid was observed. The solid showed aggregation behavior and turned into a sticky mass upon attempts to reduce the size of the powdered solid in a mortar.

Such inference was supported by slightly pink color observed during the preparation of PZQ implants using poly(ε-caprolactone) (Cheng et al., 2009). Therein, HPLC and ^{1}H NMR analyses of implants revealed that the PZQ in such products showed no modifications since no additional peaks were found. The same observations were made by Oppel on the production process of PZQ-lipid microparticles by heating the drug at 150 °C (Oppel, 2008).

A similar behavior was observed in other APIs, for example, the NSAID Piroxicam presented a bright yellow monohydrate with turned into the colorless anhydrate after dehydration (Sheth et al., 2004). On the other hand, the crystals of caffeine monohydrate also presented changes in their optical properties during dehydration due to a fast water-loss (Byrn and Lin, 1976).

3.3. Spectroscopic analysis

3.3.1. Mid-infrared

Fig. 5 shows the spectra of the solid forms in the MIR region. All PZQ forms presented main bands in the same regions.

However, three main diagnostic signals were found, in the 3500–3300 cm^{-1} interval [υ(O−H), in the 1655–1580 cm^{-1} zone [υ(C=O) and υ(C=C)] and in the 780–730 cm^{-1} [γ(C−H) aromatic C−H bending vibration] area. The list of relevant signals and their attribution is detailed in Table 1; those of PZQ-A and PZQ-AM are consistent with the literature for the corresponding solid forms (Borrego-Sánchez et al., 2017; Passerini et al., 2006).

The spectra of the three solid forms exhibited significant differences in the first zone, corresponding to the presence of water (Drozd and Daszkiewicz, 2018). As expected, PZQ-MH showed the highest peak intensity at 3417 cm^{-1}, a negligible signal in the region was found in case of PZQ-AM (Khankari and Grant, 1995), probably due to adsorbed moisture, whereas PZQ-A lacked absorption, confirming the absence of water in its structure.

In the second region, related to the amide carbonyl stretching vibration, PZQ-A exhibited a well-defined double peak at 1620 and 1647 cm^{-1}, where the first signal can be assigned to the less rigid carbonyl group that attached to the cyclohexyl ring. On the other hand, PZQ-AM showed two strongly overlapped peaks at 1632 cm^{-1} and 1639 cm^{-1} (Chaud et al., 2013). However, PZQ-MH manifested a single broad carbonyl signals at 1626 cm^{-1}.

Changes in position of the carbonyl band may reflect both, steric and electronic effects. The observed displacement toward lower wavenumbers in the PZQ-MH, when compared with PZQ-AM, may lays on the decreased electron density of the carbonyl group when C=O···H_2O H-bonds are formed or carbonyl rigidization for the same phenomenon.

However, since the band are shifted in the spectra, it is reasonable to assume that carbonyl group are involved in the new interactions, either by H-bond formation or through conformational variation. This effect may also be associated with the increased energy of the cyclohexylcarboxamide carbonyl (Espinosa-Lara et al., 2013).

The crystallization water provides hydrogen bonds to connect the carbonyl groups in the solid. It is known that in PZQ-A both carbonyl groups are oriented in a *syn* conformation (Espinosa-Lara et al., 2013), whereas in the crystal of the (*R*)-enantiomer hemihydrate, these carbonyl groups are oriented in an *anti*-conformation (Borrego-Sánchez et al., 2016). On these bases, it may be inferred that the observed changes in PZQ-MH may reflect that it suffers differences in their conformational arrangements with regards to PZQ-A, which involve at least one of the carbonyl moieties.

In the third zone, PZQ-A presented a broad peak with a shoulder at 762 cm^{-1}, contrasting with PZQ-AM, which exhibited a slim signal at 756 cm^{-1}. Both signals relate to the *ortho*-disubstituted nature of the aromatic ring moiety of the drug. On the other hand, the PZQ-MH showed peaks with similar shape, in between of the first two, at 758 and 760 cm^{-1}.

3.3.2. Near infrared

The NIR spectra of the studied solid forms in the 700–2500 nm region are shown in Fig. 6. PZQ gave a spectrum with three-weak bands at 1387 nm (first CH overtone), 1150 and 1205 nm (second CH overtone) and 2142 nm (amide combination), characteristic of an aromatic compound. In addition, combination bands of the basic CH vibration were observed at 1721–1756 nm and 2290–2440 nm, in agreement with the literature (Ibrahim and Hassan, 2001). Spectral comparison with PZQ-AM revealed some differences, mainly in the last two zones, reflecting variations among the packing interactions.

Comparison among the three solids (Table 2) revealed that combination bands assignable to the amide moiety were observed at 2170–2140 nm in all the solid forms and that they exhibited main differences in three spectral regions (1390–1480 nm, 1870–1950 nm and 2290–2450 nm). Changes in ArC−H, CH, CH_2, combination were deemed likely to result from packing changes in the lattice of the forms.

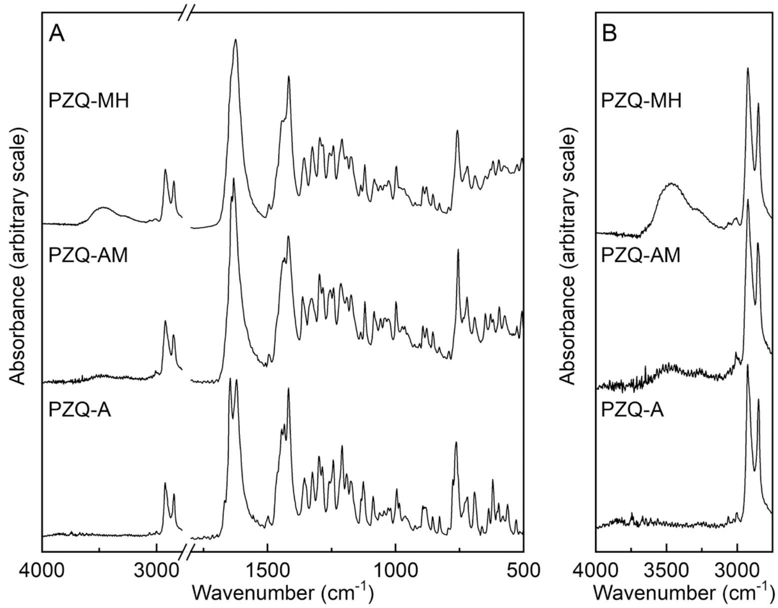

Fig. 5. MIR spectra of the solid forms of PZQ, including PZQ-A, PZQ-AM and PZQ-MH. (A) Full range (4000–500 cm^{-1}); (B) Zoom of the oxygen-hydrogen stretching [υ(OH)] region 4000–3200 cm^{-1}.

Table 1
Main absorptions of PZQ-A, PZQ-AM, and PZQ-MH in the MIR region and their attribution.

PZQ-A Signal (cm^{-1})	PZQ-AM Signal (cm^{-1})	PZQ-MH Signal (cm^{-1})	Assignment
–	–	3417	υ(OH)
2926, 2848	2924, 2854	2926, 2850	$υ_s$(CH) and $υ_{as}$(CH)
1647, 1620	1639, 1632	1626	υ(C═O); amide
1445	1431	1433	δ(C–C)
1418	1418	1417	$δ_s$(CH); cyclic structure
1300	1298	1296	υ(C–N)
1325, 1286, 1244, 1259, 1209	1327, 1284, 1255, 1248, 1215	1325, 1284, 1257, 1244, 1209	δ(C–N); axial deformation; $γ(CH)_{COCH2N}$
762	756	760	γ(CH); aromatic -CH wagging of *ortho*-disubstituted aryl

On the other hand, variations in the first two zones were attributed to the absorption of the first overtone of the stretching band of OH and to the combination of stretching and flexion bands of the OH moiety; hence, they were assigned to the water of hydration in PZQ-MH. Such changes, caused by differences in water content of the pseudo-polymorphs are diagnostic and allowed to distinguish PZQ-MH in the samples (Blanco and Villar, 2000).

3.3.3. Solid-state ^{13}C NMR

Solid-state NMR is one of the gold standard technologies to unveil the structures of polymorphs and pseudo-polymorphs. Fig. 7 shows the CP/MAS ^{13}C NMR spectra of the solid forms of PZQ, acquired with the use of the TOSS sequence.

The ^{13}C NMR signals show differences in the molecular environment. The upfield resonances (δ 24.43–51.13 ppm) were attributed to the nine CH_2 groups and methinic C13, whereas the resonances found in the range δ 54.87–57.61 ppm were assigned to C11b, the stereogenic center of PZQ.

Chemical shift variations reflect the existence of differences in packing of the molecules, whereas signal overlapping may stem from chemical shift differences between similar groups, packing issues as well as from signal broadening in the case of the amorphous materials.

The spectrum of PZQ-A exhibited more signals than the 19 carbon nuclei found in the structure of PZQ, consistent with its proposed crystal structure and with the literature (Sanchez-Guadarrama et al., 2015). Signal assignment (Table 3) was made taking into account the chemical changes of the carbon atom types and was in agreement with the literature (Sanchez-Guadarrama et al., 2015).

In fact, the amorphous form PZQ-AM exhibited broader signals of their C7-C11a aromatic carbon atoms (δ 129.43–136.93 ppm) than their crystalline congeners, and significant differences were also found among the resonances in the region attributed to the carbonyl groups (δ 161.76–174.89 ppm), in agreement with the literature.

These should result from the dissimilar ability of the carbonyls to engage in intermolecular hydrogen bonding with another molecule of PZQ or with water in case of the PZQ-MH. Although minor in intensity and affecting mainly the non-aromatic signals, differences between the spectra of PZQ-AM was also found.

On the other hand, the spectral trace of PZQ-MH suggested that the form is crystalline in nature, where the deshielding of the carbonyl carbon atoms with regards to PZQ-A may be taken as evidence of their involvement in intermolecular hydrogen bonding with the hydration

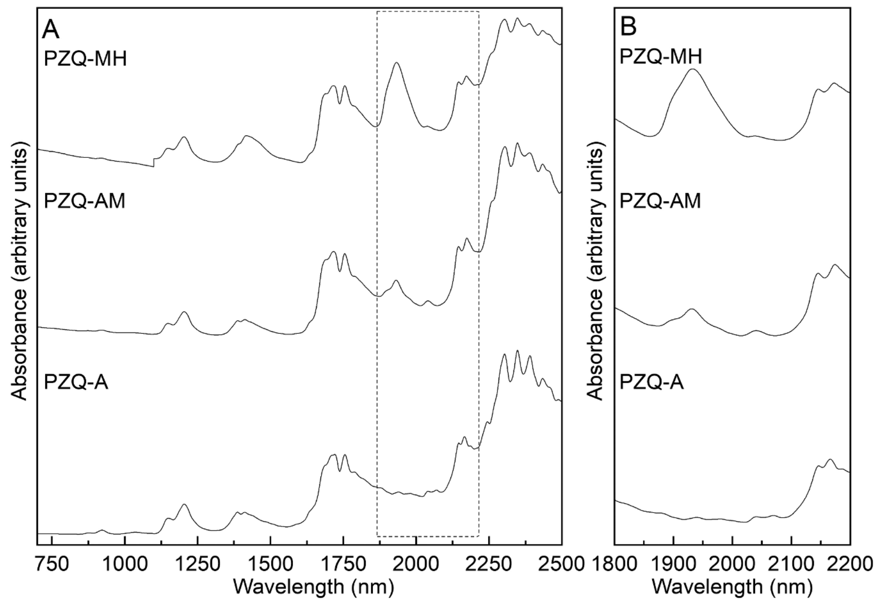

Fig. 6. NIR spectra of the solid forms of PZQ, including PZQ-A, PZQ-AM and PZQ-MH. (A) Full range (700–2500 nm); (B) Zoom of the region found in the dashed box on Fig. 6A.

Table 2
Assignment of the main NIR absorptions of PZQ-A, PZQ-AM and PZQ-MH.

PZQ-A Maximum (nm)	PZQ-AM Maximum (nm)	PZQ-MH Maximum (nm)	Assignment
907	–	–	3rd CH overtone
1150, 1205	1149, 1204	1149, 1204	2nd CH overtone
1387	1388	1393	CH; combination
–	–	1407	1st OH overtone
1678	1682	1682	ArC–H; CH_2CO
1721	1717	1717	1st CH overtone
1756	1755	1755	CH_2; combination
–	–	1926	OH stretch; combination
2142	2142	2140	Amide combination
2237	2256	2254	CH; aryl
2343	2343	2345	CH and CH_2 combinations
2428	2427	2429	CH; aryl

water, provided the PZQ-MH adopts the same conformation of PZQ-A.

3.4. Thermal analysis

Fig. 8A shows the DSC thermograms of the studied PZQ forms. The crystalline form PZQ-A showed an endothermic peak at 144 °C, correlated to its melting point. The value of ΔH_m = 91.17 J/g was in good agreement with the literature (Cugovcan et al., 2017). The shape of the curve and the transition temperature confirmed both, the chemical purity and crystallinity of the racemic sample.

On the other hand, PZQ-AM did not present a characteristic melting point, this observation was in agreement with their amorphous state, resulting from small differences between the intermolecular forces acting in the molten solid and the disordered state.

PZQ-MH exhibited two endothermic transitions; the first one, between 80 and 130 °C, was related to a dehydration event which

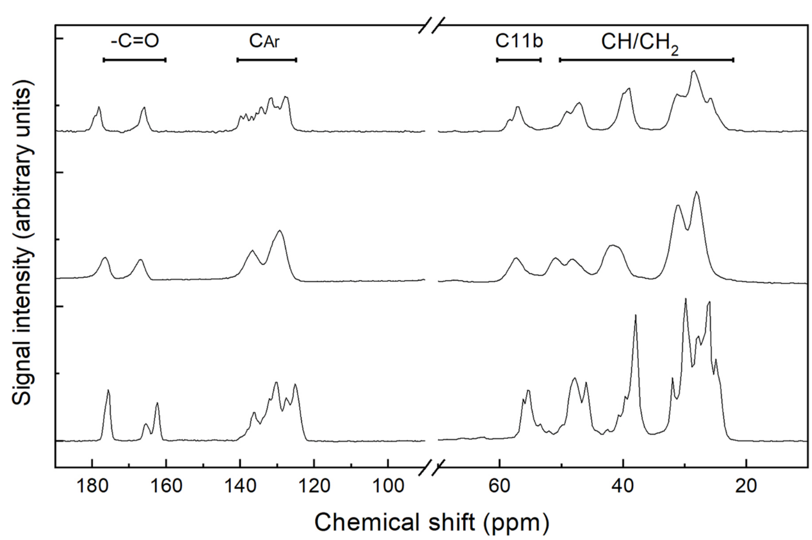

Fig. 7. CP/MAS ^{13}C NMR of PZQ-A, PZQ-AM and PZQ-MH.

Table 3
CP/MAS ^{13}C NMR chemical shift assignment for the solid forms of PZQ.

Position	PZQ-A Chemical shift (δ/ppm)	PZQ-AM Chemical shift (δ/ppm)	PZQ-MH Chemical shift (δ/ppm)
1	45.48	48.43	47.85
2	–	–	–
3	47.34	51.13	49.76
4	161.75–164.91	167.00	164.42
5	–	–	–
6	37.45–40.18	41.70	39.97
7	27.41–29.50	31.40	29.68
7a	135.55	136.93	136.41–137.60*
8	124.4–135.5	136.93	134.61–135.74*
9	124.4–135.5	129.43	129.60*
10	124.45	129.43	125.51*
11	126.97	129.43	127.82*
11a	129.56–131.50	136.93	134.93*
11b	54.84–55.67	57.61	57.61
12	174.95	176.60	177.20
13	37.48–40.16	41.70	39.97
14	31.50	31.40	31.82
15	24.46	28.34	27.02
16	25.66–29.49	28.34	28.36
17	25.66–29.49	28.34	28.36
18	25.66–29.49	31.40	31.82

*Tentative peak-assignation.

confirmed the presence of water. This was followed by an endothermic signal with a peak at 144 °C (ΔH_m = 104.13 J/g), related to the PZQ melting point as observed for PZQ-A. Such observations revealed the existence of a crystal structure that holds the water until dehydration, and undergoes phase transformation to the anhydrous form up to the fusion event.

The endothermic transitions experienced for PZQ-A and PZQ-MH were in agreement with those observed in the melting point apparatus. On the other hand, PZQ-AM lacked a well-defined melting event, in conformity with the literature (Costa et al., 2016).

The analysis of the TGA curve (Fig. 8B) of PZQ-A revealed that the initial mass of drug remained stable (± 0.25%) up to the fusion process at 144 °C, whereas the loss of mass started around 40 °C and continued gradually until 140 °C in the other samples. PZQ-AM experienced a small loss of mass (0.8% *w/w*) associated with the evaporation of adsorbed water, this is in line with the higher hygroscopicity exhibited by amorphous in comparison to their crystalline forms and resulting in the first ones immediately hydrated in contact to the air moisture.

Contrarily, the total water weight loss was 5.4% *w/w* for PZQ-MH (99.1% of the theoretical amount of 5.45% *w/w*), evidencing a major transition in the range 80–120 °C, followed by a plateau up to the fusion event. An additional assessment of the water content of PZQ-MH was performed through the official USP loss on drying test (Tode et al., 2009), at 105 °C up to constant weight (3 h), where the sample experienced a weight loss of 94.6% with regards to the theoretical amount. This result confirmed the stoichiometry of PZQ-MH as PZQ.H_2O.

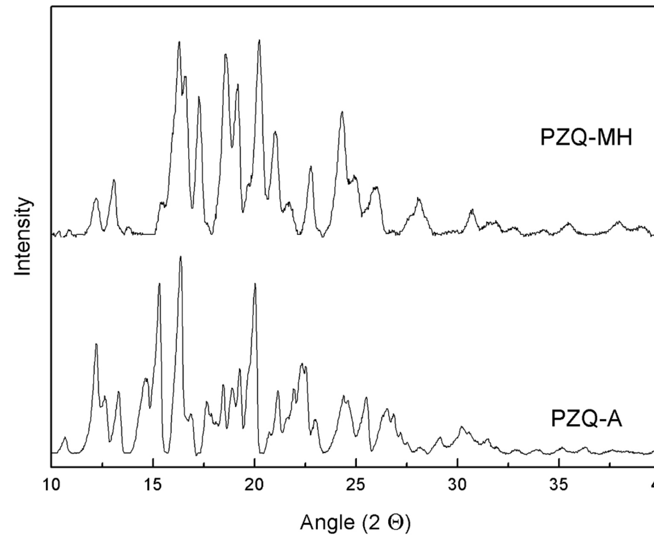

Fig. 9. Powder X-ray diffraction patterns of PZQ-A and PZQ-MH.

3.5. Analysis of XRPD

In order to further assess the identity and crystallinity of the new form, XRPD studies were carried out with PZQ-MH and the results were compared with those obtained for PZQ-A and PZQ-AM.

The X-ray powder diffraction pattern of the PZQ-A recorded at room

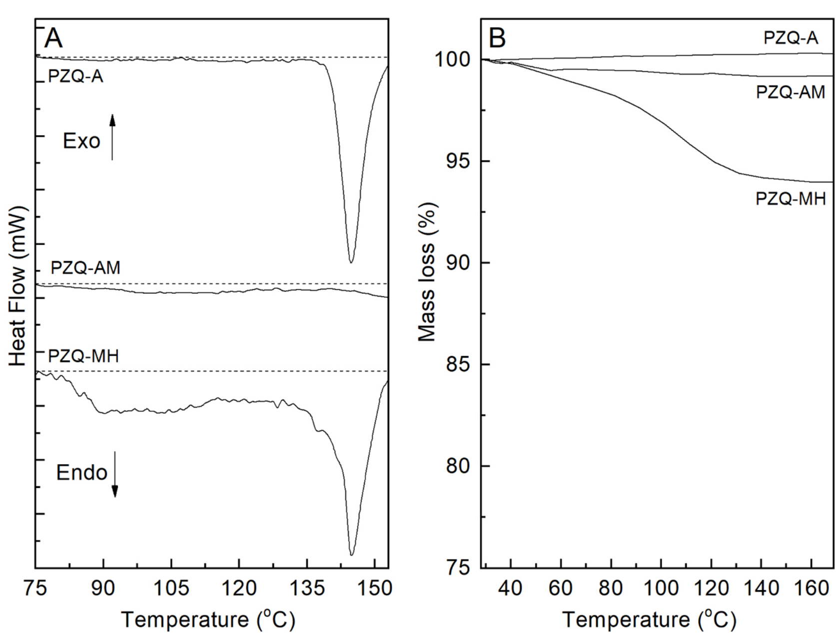

Fig. 8. Thermal analysis of the studied forms of PZQ. (A) DSC thermograms. (B) TGA curves.

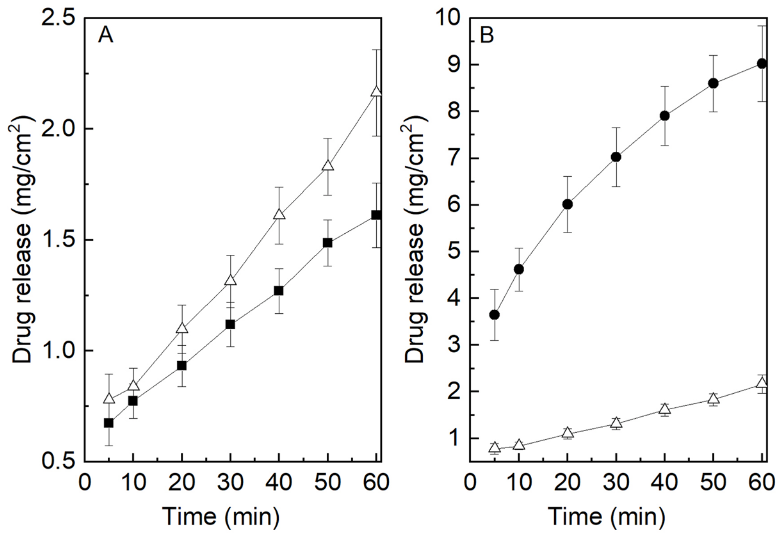

Fig. 10. Intrinsic dissolution rates of the solid forms, (A) PZQ-MH (Δ) and PZQ-A (■), and (B) PZQ-MH (Δ) and PZQ-AM (●).

temperature (Fig. 9), shows sharp peaks, confirming the crystallinity of the sample. Majors diffraction peaks were found at 2 Θ degree of 12.1, 13.2, 14.7, 13.3, 16.3, 17.5, 18.5, 18.8, 19.2, 20.0, 21.1, 21.7, 22.5, 22.9, 24.3, 25.4, 26.5, 28.8, 29.1, 30.1 and 31.4. The peak positions were in agreement with literature (Espinosa-Lara et al., 2013; Zanolla et al., 2018).

The diffraction pattern of the PZQ-MH shows sharp and well-defined peaks indicating the crystallinity of the new sample. In addition, clear differences were found among both species PZQ-A and PZQ-MH during the comparison of diffraction patterns, confirming that both are different. Diagnostic signals for PZQ-MH were found at 2 Θ degree of 12.0, 13.0, 16.2, 17.2, 18.5, 19.1, 20.2, 21.0, 22.7, 24.7, 24,9 26.6, 28.0 and 30.7.

Finally, PZQ-AM did not show any diffraction signals but an amorphous halo, as expected for amorphous form.

3.6. Intrinsic dissolution rate

The IDR is a standardized kinetic method, which involves the determination of the dissolution rate of pure substances after compaction, under constant surface conditions. The IDR evaluation of the PZQ solid forms was carried out in order to perform a functional assessment of the potential biopharmaceutical properties of the new form and to compare their performance with related solids.

Fig. 10.A displays the IDR results of the three studied forms in water, for 60 min. It was observed that the dissolution of PZQ-A is slow (1.6 mg cm^{-2} h^{-1}) and incomplete in the studied time range, which is in agreement with its low oral bioavailability. On the other hand, the monohydrate exhibited a value of 2.2 mg cm^{-2} h^{-1}, a slightly higher dissolution rate than PZQ-A

Curiously, the higher dissolution rates of the hydrates compared to PZQ-A are somehow contrary to expectations for hydrates, which are usually less soluble than the corresponding anhydrous drugs. However, Savjani and coworkers proposed a crystal engineering approach involving the preparation of hydrates and solvates as a non-common but suitable strategy for enhancing the dissolution rate (Savjani et al., 2012).

A similar behavior was found by Kadrate and Bavitz for Norfloxacin, which showed higher and maintained dissolution rates for its hydrate forms than the anhydrate or partially anhydrate substance (Katdare and Bavitz, 1984). Additionally, Erythromycin dihydrate also exhibited significantly higher dissolution rate when compared to its monohydrate and anhydrate forms (Allen et al., 1978).

Franklin and co-workers elaborated a model to predict the hydrates solubilities (Franklin et al., 2016). This model takes into account the dehydration entropy and crystal lattice energy as major variables. Thus, if the crystal phase in the hydrate and the anhydrate are not the same, the solubility of a hydrate may be similar or higher than of the solubility of the initial anhydrous form. This fact could be explained since the crystal phase obtained after a "theoretical dehydration" process could show lower crystal enthalpy than the original anhydrous phase.

Finally, PZQ-AM showed the highest dissolution rate (9.0 mg cm^{-2} h^{-1}, Fig. 10.B) consistently with its nature, four-folding that of PZQ-MH (2.2 mg cm^{-2} h^{-1}).

4. Conclusions

The preparation of the monohydrate (PZQ-MH) as a new solid form of PZQ is reported. The form was characterized and compared with the known commercial polymorph and the amorphous drug. ^{1}H NMR in solution was used to assess the integrity of PZQ after the preparation of the solid forms, whereas vibrational spectroscopies (MIR and NIR) and thermal analyses (DSC and TGA) revealed the differences stemming from the water content and crystalline nature of the new form. Additionally, ssNMR spectroscopy also provided concluding evidence of the formation of the new solid form and evidenced differential characteristics from PZQ-A and PZQ-AM. Finally, XRPD studies demonstrated that PZQ-MH is a crystalline phase, which exhibited a distinctive and unique diffraction pattern than PZQ-A.

Intrinsic dissolution studies were carried out as a functional test and minor differences were found between the dissolution rate properties of PZQ-MH and PZQ-A.

Collectively analyzed, the results of the microscopic, spectroscopic, thermal, difractometric and functional analyses unequivocally confirm the formation of a new phase, which is the pseudo-polymorphic form PZQ-MH. The characterization of the new solid adds to the current knowledge of PZQ and may have impact in the development of new and improved functional derivatives of the API.

Acknowledgements

The authors gratefully acknowledge the financial support received from Consejo Nacional de Investigaciones Científicas y Técnicas (CONICET; PUE IQUIR 2016) and Secretaría de Ciencia y Tecnología de la UNR (SECyT-UNR, Projects BIO300 and BIO498). The Agencia Santafesina de Ciencia, Tecnología e Innovación (ASACTeI) for awarding the institutional grant AC-2015-0005 (400 MHz NMR machine). The authors also thank IFIR (CONICET-UNR) for granting access to the TG equipment. D.S.R. also thanks CONICET for her fellowship.

References

Allen, P.V., Rahn, P.D., Sarapu, A.C., Vanderwielen, A.J., 1978. Physical characterization of erythromycin: anhydrate, monohydrate, and dihydrate crystalline solids. J. Pharm. Sci. 67, 1087–1093. https://doi.org/10.1002/jps.2600670816.

Arrúa, E.C., Ferreira, M.J.G., Salomon, C.J., Nunes, T.G., 2015. Elucidating the guest-host interactions and complex formation of praziquantel and cyclodextrin derivatives by 13C and 15 N solid-state NMR spectroscopy. Int. J. Pharm. 496, 812–821. https://doi.org/10.1016/j.ijpharm.2015.11.026.

Blanco, M., Valdés, D., Llorente, I., Bayod, M., 2005. Application of NIR spectroscopy in polymorphic analysis: study of pseudo-polymorphs stability. J. Pharm. Sci. 94, 1336–1342. https://doi.org/10.1002/jps.20362.

Blanco, M., Villar, A., 2000. Polymorphic analysis of a pharmaceutical preparation by NIR spectroscopy. Analyst 125, 2311–2314. https://doi.org/10.1039/b005746k.

Borrego-Sánchez, A.M., 2018. Interaction of Praziquantel With Micro- and Nanostructured Inorganic Excipients. University of Granada.

Borrego-Sánchez, A., Hernández-laguna, A., Sainz-díaz, C.I., 2017. Molecular modeling and infrared and Raman spectroscopy of the crystal structure of the chiral anti-parasitic drug praziquantel. J. Mol. Model. 23, 106. https://doi.org/10.1007/s00894-017-3266-3.

Borrego-Sánchez, A., Viseras, C., Aguzzi, C., Sainz-Díaz, C.I., 2016. Molecular and crystal structure of praziquantel. Spectroscopic properties and crystal polymorphism. Eur. J. Pharm. Sci. 92, 266–275. https://doi.org/10.1016/j.ejps.2016.04.023.

Bygott, J.M., Chiodini, P.L., 2009. Praziquantel: neglected drug? Ineffective treatment? Or therapeutic choice in cystic hydatid disease? Acta Trop 111, 95–101. https://doi.org/10.1016/j.actatropica.2009.04.006.

Bylund, G., Bång, B., Wikgren, K., 1977. Tests with a new compound (Praziquantel) against diphyllobothrium latum. J. Helminthol. 51, 115–119. https://doi.org/10.1017/S0022149X00007343.

Byrn, S.R., Lin, C.T., 1976. The effect of crystal packing and defects on desolvation of hydrate crystals of caffeine and L-(-)-1,4-cyclohexadiene-1-alanine. J. Am. Chem. Soc. 98, 4004–4005. https://doi.org/10.1021/ja00429a048.

Cedillo-Cruz, A., Aguilar, M., Flores-Alamo, M., Palomares-Alonso, F., Jung-Cook, H., 2013. A straightforward and efficient synthesis of praziquantel enantiomers and their 4 0 -hydroxy derivatives. Tetrahedron 25, 133–140. https://doi.org/10.1016/j.tetasy.2013.11.004.

Chaud, M.V., Lima, A.C., Vila, M.M.D.C., Paganelli, M.O., Paula, F.C., Pedreiro, L.N., Gremião, M.P.D., 2013. Development and evaluation of praziquantel solid dispersions in sodium starch glycolate. Trop. J. Pharm. Res. 12, 163–168. https://doi.org/10.4314/tjpr.v12i2.5.

Cheng, L., Guo, S., Wu, W., 2009. Characterization and in vitro release of praziquantel from poly (ε -caprolactone) implants. Int. J. Pharm. 377, 112–119. https://doi.org/10.1016/j.ijpharm.2009.05.007.

Coeli, R., Baba, E.H., Araujo, N., Coelho, P.M.Z., Oliveira, G., 2013. Praziquantel treatment decreases schistosoma mansoni. genetic diversity in experimental infections. PLoS Negl. Trop. Dis. 7. https://doi.org/10.1371/journal.pntd.0002596.

Costa, E.D., Priotti, J., Orlandi, S., Leonardi, D., Lamas, M.C., Nunes, T.G., Diogo, H.P., Salomon, C.J., Ferreira, M.J., 2016. Unexpected solvent impact in the crystallinity of praziquantel/poly(vinylpyrrolidone) formulations. A solubility, DSC and solid-state NMR study. Int. J. Pharm. 511, 983–993. https://doi.org/10.1016/j.ijpharm.2016.08.009.

Cugovcan, M., Jablan, J., Jug, M., 2017. Biopharmaceutical characterization of praziquantel cocrystals and cyclodextrin complexes prepared by grinding. J. Pharm. Biomed. Anal. 137, 42–53.

da Silva, V.B.R., Campos, B.R.K.L., de Oliveira, J.F., Decout, J.L., do Carmo Alves de Lima, M., 2017. Medicinal chemistry of antischistosomal drugs: praziquantel and oxamniquine. Bioorg. Med. Chem. 25, 3259–3277. https://doi.org/10.1016/j.bmc.2017.04.031.

Drozd, M., Daszkiewicz, M., 2018. A synthesis, X-ray crystallographic and vibrational studies of guanidinium o-nitrobenzoate hydrate. New NLO crystal in guanidinium nitrobenzoate family. J. Mol. Struct 1161, 383–392. https://doi.org/10.1016/j.molstruc.2018.02.077.

El-subbagh, H.I., Al-badr, A.A., 1998. Anal. Profiles Drug Subst. Excip 25, 463.

Espinosa-Lara, J.C., Guzman-Villanueva, D., Arenas-Garc, I., Herrera-Ruiz, D., Roma, P., Morales-Rojas, H., Ho, H., 2013. Cocrystals of active pharmaceutical Ingredients-Praziquantel in combination with oxalic, malonic, succinic, maleic, fumaric, glutaric, adipic, and pimelic acids. Cryst. Growth Des. 13, 169–185.

Franklin, S.J., Younis, U.S., Myrdal, P.B., 2016. Estimating the aqueous solubility of pharmaceutical hydrates. J. Pharm. Sci. 105, 1914–1919. https://doi.org/10.1016/j.xphs.2016.03.040.

Gonzales-Esquivel, D., Rivera, J., Castro, N., Yepez-Mulia, L., Helgi, J., 2005. In vitro characterization of some biopharmaceutical properties of praziquantel. Int. J. Pharm. 295, 93–99. https://doi.org/10.1016/j.ijpharm.2005.01.033.

Gottlieb, H.E., Kotlyar, V., Nudelman, A., 1997. NMR chemical shifts of common laboratory solvents as trace impurities. J. Org. Chem. 62, 7512–7515. https://doi.org/10.1021/jo971176v.

Ibrahim, H.H, Hassan, H.N, 2001. Near Infra red reflectance spectroscopic determination of praziquantel. Anal. Sci. 17, i69–i71.

Katdare, A.V., Bavitz, J.F., 1984. Hydrate related dissolution characteristics of norfloxacin A. Drug Dev. Ind. Pharm. 10, 789–807.

Khankari, R.K., Grant, D.J.W., 1995. Pharmaceutical hydrates. Thermochim. Acta 248, 61–79. https://doi.org/10.1016/0040-6031(94)01952-D.

Kolenyak-Santos, F., Garnero, C., De Oliveira, R.N., de Souza, A.L.R., Chorilli, M., Allegretti, S.M., Longhi, M.R., Chaud, M.V., Gremião, M.P.D., 2015. Nanostructured lipid carriers as a strategy to improve the in vitro schistosomiasis activity of praziquantel. J. Nanosci. Nanotechnol. 15, 761–772. https://doi.org/10.1166/jnn.2015.9186.

Leopold, G., Ungethum, W., Groll, E., Diekmann, H.W., Nowak, H., Wegner, D.H., 1978. Clinical pharmacology in normal volunteers of praziquantel, a new drug against schistosomes and cestodes. An example of a complex study covering both tolerance and pharmacokinetics. Eur. J. Clin. Pharmacol. 14, 281–291. https://doi.org/10.1007/bf00560463.

Liu, Y., Wang, X., Wang, J.K., Ching, C.B., 2004. Structural characterization and enantioseparation of the chiral compound praziquantel. J. Pharm. Sci. 93, 3039–3046. https://doi.org/10.1002/jps.20211.

Management Sciences for Health, World Health Organization, 2011. International drug price indicator guide. Management sciences for health. Cambridge USA, Cambridge (USA). 10.1017/CBO9781107415324.004.

Mari, L., Ciddio, M., Casagrandi, R., Perez-Saez, J., Bertuzzo, E., Rinaldo, A., Sokolow, S.H., De Leo, G.A., Gatto, M., 2017. Heterogeneity in schistosomiasis transmission dynamics. J. Theor. Biol. 432, 87–99. https://doi.org/10.1016/j.jtbi.2017.08.015.

Meister, I., Kovac, J., Duthaler, U., Odermatt, P., Huwyler, J., 2016. Pharmacokinetic study of praziquantel enantiomers and its main metabolite R- trans -4-OH-PZQ in plasma, blood and dried blood spots in opisthorchis viverrini-. Infected Patients 1–15. https://doi.org/10.1371/journal.pntd.0004700.

Meyer, T., Sekljic, H., Fuchs, S., Bothe, H., Schollmeyer, D., Miculka, C., 2009. Taste, a new incentive to switch to (R) -Praziquantel in schistosomiasis treatment. PLoS Negl. Trop. Dis. 3, 3–7. https://doi.org/10.1371/journal.pntd.0000357.

Oppel, K., 2008. Taste Masking of an Active Pharmaceutical Ingredient For Veterinary Application. University of Basel.

Passerini, N., Albertini, B., Perissutti, B., Rodriguez, L., 2006. Evaluation of melt granulation and ultrasonic spray congealing as techniques to enhance the dissolution of praziquantel. Int. J. Pharm. 318, 92–102. https://doi.org/10.1016/j.ijpharm.2006.03.028.

Sánchez-Guadarrama, O., Mendoza-Navarro, F., Cedillo-Cruz, A., Jung-Cook, H., Arenas-García, I., Delgado-Díaz, A., Herrera-Ruiz, D., Morales-Rojas, H., Höpfl, H., 2015. Chiral resolution of RS -Praziquantel via diastereomeric co-crystal pair formation with L - Malic Acid. Cryst. Growth Des. 16, 307–314. https://doi.org/10.1021/acs.cgd.5b01254.

Savjani, K.T., Gajjar, A.K., Savjani, J.K., 2012. Drug solubility: importance and enhancement techniques. ISRN Pharm. 2012, 1–10. https://doi.org/10.5402/2012/195727.

Sheth, A.R., Zhou, D., Muller, F.X., Grant, D.J.W., 2004. Dehydration kinetics of piroxicam monohydrate and relationship to lattice energy and structure. J. Pharm. Sci. 93, 3013–3026. https://doi.org/10.1002/jps.20191.

Tode, C., Takeuchi, A., Iwakawa, S., Tatsumi, A., Sugiura, M., 2009. Hydrogen–Deuterium (H–D) exchange reaction of warfarin in D2O solution. Chem. Pharm. Bull. 57, 653–656.

Toro, R., Kaduk, J, Delgado, M, de D, G.D, 2014. Structural characterization of praziquantel: a broad spectrum anthelmintic, in powder diffraction. Powder Diffr. 29, 206–207.

United States Pharmacopeia Convention, 2015. United states pharmacopeia and national formulary (USP 39–NF 34). Rockville.

Witzleb, R., Kanikanti, V., Hamann, H., Kleinebudde, P., 2011. Influence of needle-shaped drug particles on the solid lipid extrusion process. Powder Technol. 207, 407–413. https://doi.org/10.1016/j.powtec.2010.11.027.

Woelfle, M., Seerden, J., Gooijer, J.De, Pouwer, K., Olliaro, P., Matthew, H., 2011. Resolution of praziquantel. PLoS Negl. Trop. Dis. 5, e1260. https://doi.org/10.1371/journal.pntd.0001260.

World Health Organization, 2008. WHO model list of essential medicines.

World Health Organization, 2019. Schistosomiasis [WWW document]. fact sheet n 115.

Zanolla, D., Perissutti, B., Passerini, N., Chierotti, M.R., Hasa, D., Voinovich, D., Gigli, L., Demitri, N., Geremia, S., Keiser, J., Cerreia Vioglio, P, Albertini, B, 2018. A new soluble and bioactive polymorph of praziquantel. Eur. J. Pharm. Biopharm. 127, 19–28. https://doi.org/10.1016/j.ejpb.2018.01.018.